When is a Vertex not a Vertex? An Analysis of the Structures of $[MB_{10}H_{12}]$ Metallaboranes†

Stuart A. Macgregor, Andrew J. Wynd, Nicola Moulden, Robert O. Gould, Paul Taylor, Lesley J. Yellowlees and Alan J. Welch*

Department of Chemistry, University of Edinburgh, West Mains Road, Edinburgh EH9 3JJ, UK

There are two extreme descriptions of the bonding between metal fragments and the $\{B_{10}H_{12}\}$ ligand. In the first the metal is regarded as a full cluster vertex in an 11 vertex *nido* metallaborane; the B_{10} residue is formally *arachno*-$\{B_{10}H_{12}\}^{4-}$. In the second the metal is a poor cluster vertex and does not significantly perturb the borane fragment architecture, formally *nido*-$\{B_{10}H_{12}\}^{2-}$. *nido*-$\{B_{10}H_{12}\}^{2-}$ and *arachno*-$\{B_{10}H_{12}\}^{4-}$ have exactly the same pattern of connectivities, but their structures may be distinguished by *root mean square* (*r.m.s.*) *misfit* calculations. Applications of these calculations to $[MB_{10}H_{12}]$ metallaboranes reveals clear examples of both extreme formalisms, and in $[(C_6H_{11})_3PAuB_{10}H_{12}]^-$ and $[(OC)_3CoB_{10}H_{12}]^-$ the formal metal oxidation states (Au^+, Co^{3+}) that follow directly from these descriptions of the $\{B_{10}H_{12}\}$ ligand agree well with independent measurement. In addition, however, several metallaboranes are found to have structures in which the B_{10} residue lies between that of $\{B_{10}H_{12}\}^{2-}$ and $\{B_{10}H_{12}\}^{4-}$. The *verticity* of a metal fragment is introduced as a convenient way of describing its relative degree of incorporation into the metallaborane as a true cluster vertex. By analysis of the results of extended-Hückel molecular orbital–fragment molecular orbital (EHMO–FMO) calculations verticity is found, to a first approximation, to be directly related to the number of available valence orbitals the metal fragment possesses. Metal fragments that are one-orbital sources are poor vertices, whilst those that are three-orbital sources are good vertices, but the boundary between good- and poor-metal vertex is not well defined and there is, in essence, a continuum of verticity.

Metallaboranes in which the borane fragment is present as $\{B_{10}H_{12}\}$ (or a simple derivative thereof) constitute a substantial group, and are known both as main-group and transition-metal complexes. In a recent review of polyhedral metallaboranes Kennedy[1] has pointed out that, with only one exception, the connectivity pattern of this group is that shown in **I**, *i.e.* metal and bridging H atoms in non-adjacent positions in the open face of the polyhedron.

If one assumes that **I** has a *nido* icosahedral cage architecture and adopts the conventional numbering system for such a species (**Ia**), the metal atom is at position 7 and the μ-H atoms bridge the B(8)–B(9) and B(10)–B(11) edges. Such a description implies a true heteroborane, *i.e.* the metal atom is regarded as a full polyhedral vertex. Here the geometry of the $\{B_{10}H_{12}\}$ subunit is that of **II**, the *arachno* fragment $\{B_{10}H_{12}\}^{4-}$.

However, an alternative description of **I** is possible—that in which the metallaborane is viewed essentially as a complex between a metal ion and *nido*-$\{B_{10}H_{12}\}^{2-}$, **III**, and in which the metal is *not* formally considered as a cluster vertex. In this description (**Ib**) the boron atoms are numbered as in $B_{10}H_{14}$,[2] with μ-H atoms on the B(6)–B(7) and B(8)–B(9) edges, and with the metal atom bridging the B(6)–B(5)–B(10)–B(9) trapezium.

The distinction between the cage geometries of **II** and **III** is subtle but important. Structurally they are very little different—the pattern of connectivities is, in fact, exactly the same in both. However, **II** is correctly described as an *arachno* fragment of an icosahedron and is characterised by 13 skeletal electron pairs (s.e.p.s), whereas **III**, a *nido* fragment of an octadecahedron, has only 12 s.e.p.s associated with cluster bonding.[3] Thus, although

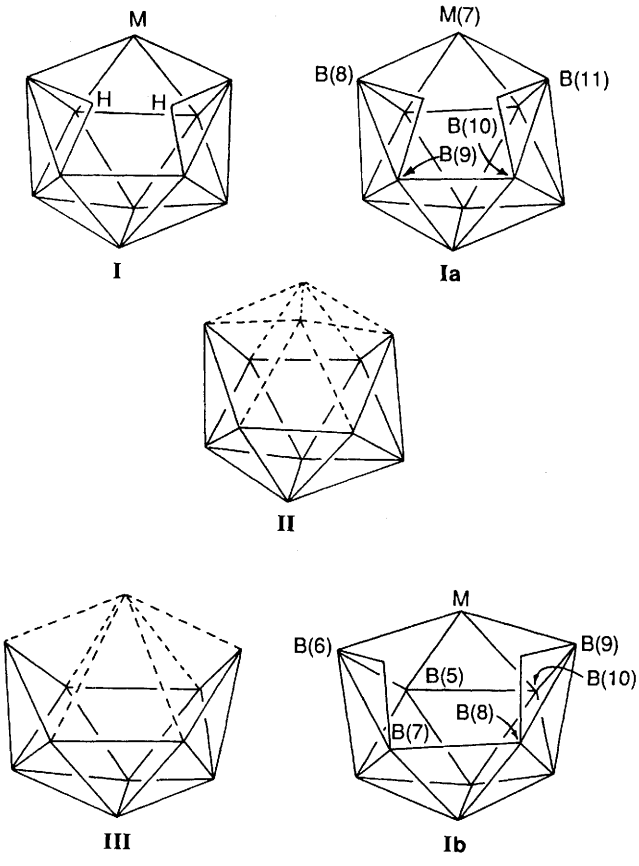

II and **III** are *geometrically* similar, they are *electronically* different, formally existing as $\{B_{10}H_{12}\}^{4-}$ and $\{B_{10}H_{12}\}^{2-}$ respectively. Amongst other things this difference has a major

† *Supplementary data available* (No. SUP 56857, 9 pp.): a listing of the source program IDEAL including sample input and output. See Instructions for Authors, *J. Chem. Soc., Dalton Trans.*, 1991, Issue 1, pp. xviii–xxii.

Non-SI unit employed: eV ≈ 1.60 × 10^{-19} J.

Table 1 A listing of metal atomic orbital parameters with exponents (ζ) and coefficients (c) for the double ζ functions of the d orbitals

Atom	Orbital	H_{ii}/eV	ζ_1	ζ_2	c_1	c_2
Au (in 1′)	6s	−10.37	2.602			
	6p	−5.35	2.504			
	5d	−13.44	6.163	2.794	0.644 18	0.535 58
Ir (in 2′)	6s	−10.18	2.500			
	6p	−5.73	2.200			
	5d	−10.09	5.796	2.557	0.635 06	0.555 61
Ir (in 3′)	6s	−9.31	2.500			
	6p	−5.73	2.200			
	5d	−8.97	5.796	2.557	0.635 06	0.555 61
Tl (in **4**)	6s	−14.80	2.300			
	6p	−11.36	1.600			
Au (in 5′)	6s	−11.24	2.602			
	6p	−6.02	2.504			
	5d	−14.65	6.163	2.794	0.644 18	0.535 58

consequence on the formal oxidation state of the bound metal atom.

Kennedy[1] has suggested that a perceptible structural difference between the B_{10} fragments of **II** and **III** in metallaboranes is often detectable, and that this can aid formal classification of the metallaborane as either **Ia** or **Ib**. He describes all main-group $[MB_{10}H_{12}]$ species as **Ib** since structural studies generally show that the long (*ca.* 2 Å) B(5)–B(10) and B(7)–B(8) connectivities of $B_{10}H_{14}$ are retained in these metallaboranes. The analysis often gains support from the recognition of broad similarities between the ^{11}B NMR chemical shifts of such species and $B_{10}H_{14}$. In contrast, in 'well behaved' transition-metal $[MB_{10}H_{12}]$ species the B(2)–B(3) and B(9)–B(10) connectivities [those corresponding to B(5)–B(10) and B(7)–B(8) in decaborane] are measurably shorter than 2 Å. Accordingly, metallaboranes of this type are properly described by **Ia**. Kennedy[1] further suggests that in **Ib** the main-group metal atom utilises two orbitals in bonding to the B_{10} polyhedron, whereas in **Ia** the transition-metal atom provides three orbitals for cluster bonding.

Delineation of metallaborane types in this way was perceptive, but has severe limitations. First, the approach is based on only two measured distances (or, put another way, the coordinates of only four of the ten boron atoms available). The use of ^{11}B NMR shifts has not been analytical. Secondly, no attempt has so far been made to validate the method by independent measurement of the metal oxidation states that are so consequent upon it. Thirdly, whilst the simple idea of main-group metal atoms as two-orbital donors and well behaved transition-metal atoms as three-orbital donors is attractive and, within the limitations of a localised orbital terminology, almost certainly correct for many $[MB_{10}H_{12}]$ metallaboranes, we will present evidence for a *continuum* of metal orbital contribution including at least one example of a *one*-orbital contribution from a metal fragment. It is important to note that the formal orbital (as well as electronic) contribution of transition-metal fragments in metallaboranes is a topic of current interest.[4]

In this paper we utilise a way of fitting the *entire* B_{10} fragment of $[MB_{10}H_{12}]$ species to unambiguous and experimentally characterised $\{B_{10}H_{12}\}^{2-}$ or $\{B_{10}H_{12}\}^{4-}$ fragments. The results reveal evidence for a continuum of metallaborane type between and including the extremes represented by **Ia** and **Ib**. We validate the method by demonstrating good internal fits between several examples of known $\{B_{10}H_{12}\}^{2-}$ fragments and between several examples of known $\{B_{10}H_{12}\}^{4-}$ fragments, with poor fits between the two sets. We show that the method applied to metallaboranes yields formal metal oxidation states that agree well with independent measurement where this is possible. We then link the continua of metallaborane type and metal orbital contribution by an analysis of the metal–cage bonding in $[MB_{10}H_{12}]$ species based upon the frontier orbitals of the appropriate metal and borane fragments.

Method

1. Root Mean Square Misfit Calculations.—These were performed with the computer program IDEAL.* This program is designed to find the closest fit between two sets of atomic coordinates containing at least three atoms common to both sets. This is accomplished by translating and rotating the second set to minimise $\Sigma\delta_i^2$, where δ_i is the distance between two corresponding atoms. Input may either be as orthogonal Å coordinates or as fractional coordinates with cell data from a crystal structure, and the second set is converted into the reference framework of the first. For the application described herein, comparison was made of pairs of sets of atomic coordinates of ten boron atoms from a variety of boranes and metallaboranes studied crystallographically. In all cases the models were adjusted to full molecular symmetry if this was not already crystallographically imposed.

To achieve an initial fit, the first set is converted to an orthogonal Å system with the origin at its centre of gravity. It is then rotated to make the atom furthest from the origin coincident with the positive z axis, and the atom furthest from that axis lie in the xz plane with a positive x coordinate. The second set is then treated similarly, using the corresponding atoms to define the positive z and x directions. An iterative least-squares procedure is then employed to rotate the second set about the x, y and z axes to minimize $\Sigma\delta_i^2$. Convergence usually occurs in about three cycles, and typically gives a *root mean square* (*r.m.s.*) *misfit*, defined by $[\Sigma_i(\delta^2)/n]^{\frac{1}{2}}$, of less than 1 Å for structurally similar groups of n atoms. Significantly poorer fits often occur when the second set is the enantiomer of the first. In this case the instruction INVERT will generate the enantiomer of the second set and try to fit it instead to the first set. On convergence, δ is given for each pair of atoms as well as the r.m.s. misfit for the two sets. The second coordinate set is then back transformed to the original coordinate system of the first.

2. Extended Hückel Molecular Orbital Calculations.—Extended Hückel molecular orbital–fragment molecular orbital (EHMO–FMO) calculations[5] were performed using a locally modified version of ICON8[6] and the modified Wolfsberg–Helmholtz formula.[7] Values of H_{ii} for metal atoms were charge iterated according to $H_{ii} = -\text{VSIE(Q)}$ where VSIE(Q) = valence state ionisation energy of orbital i when the atom has total charge Q using three VSIE(Q) functions, and since it is important in a series of such calculations in which there is charge iteration to keep the overall charge on the complex constant, we chose to study a series of monoanionic metallaboranes, as follows: $[(C_6H_{11})_3PAuB_{10}H_{12}]^-$ **1**[8] modelled by $[H_3PAuB_{10}H_{12}]^-$ **1′**, $[(Me_2PhP)_2PtB_{10}H_{12}]$ **2**[9] modelled by $[(H_3P)_2IrB_{10}H_{12}]^-$ **2′**, $[(Me_2PhP)_3PtB_{10}H_{12}]$ **3**[10] modelled by $[(H_3P)_3IrB_{10}H_{12}]^-$ **3′**, $[Me_2TlB_{10}H_{12}]^-$ **4**[11] and $[Pt(B_{10}H_{12})_2]^{2-}$ **5**[12] modelled by $[Au(B_{10}H_{12})_2]^-$ **5′**.

For the purpose of the FMO calculations the metallaboranes were each partitioned into $\{B_{10}H_{12}\}^{2-}$ and the appropriate monocationic metal fragment. Values of H_{ii} and Slater exponents for B, H, P and C were those inlaid in ICON8 (no P 3d orbitals were included). Orbital exponents and optimised H_{ii} values for metal atoms are given in Table 1. For **5′** all atomic coordinates were taken from the X-ray crystallography study of **5**. Non-hydrogen atom coordinates for **1′**–**3′** were those of the corresponding atoms of **1**–**3**, and PH_3 groups were generated with P–H 1.42 Å, M–P–H = H–P–H 109.47°. In **4** H atoms of the methyl groups were generated, C–H 1.08 Å, M–C–H =

* A copy of the program IDEAL is available as SUP 56857 or may be obtained directly from R. O. Gould, University of Edinburgh, *via* electronic mail (R.Gould@uk.ac.ed).

Table 2 Root mean square misfits (Å) between boranes and substituted boranes containing *nido*-$\{B_{10}H_{12}\}^{2-}$ and *arachno*-$\{B_{10}H_{12}\}^{4-}$ fragments*

Systems	R.m.s. misfit	δ_a	δ_b	δ_c	δ_d	δ_e	δ_f	δ_g	δ_h	δ_i	δ_j
6/7	0.074	0.145	0.034	0.037	0.151	0.045	0.046	0.045	0.032	0.034	0.016
6/8	0.059	0.046	0.106	0.073	0.063	0.044	0.036	0.031	0.045	0.071	0.030
6/9	0.026	0.018	0.012	0.009	0.023	0.018	0.009	0.066	0.009	0.023	0.018
7/8	0.067	0.104	0.086	0.098	0.088	0.052	0.019	0.024	0.015	0.067	0.023
7/9	0.080	0.151	0.026	0.033	0.132	0.056	0.052	0.109	0.025	0.056	0.029
8/9	0.067	0.059	0.104	0.075	0.045	0.060	0.040	0.095	0.039	0.074	0.035
10/11	0.052	0.084	0.089	0.024	0.024	0.058	0.045	0.045	0.032	0.032	0.020
6/10	0.199	0.377	0.377	0.123	0.123	0.164	0.076	0.076	0.137	0.137	0.081
6/11	0.166	0.297	0.297	0.116	0.116	0.108	0.113	0.113	0.112	0.112	0.101
7/10	0.181	0.290	0.371	0.112	0.140	0.132	0.086	0.042	0.161	0.127	0.078
7/11	0.146	0.202	0.293	0.100	0.124	0.078	0.107	0.074	0.138	0.100	0.098
8/10	0.206	0.338	0.413	0.168	0.110	0.143	0.075	0.045	0.175	0.183	0.093
8/11	0.176	0.225	0.346	0.168	0.095	0.087	0.102	0.084	0.153	0.160	0.111
9/10	0.209	0.390	0.377	0.129	0.127	0.180	0.073	0.139	0.143	0.151	0.098
9/11	0.178	0.310	0.297	0.120	0.117	0.124	0.112	0.178	0.119	0.129	0.118

* **6** is $B_{10}H_{14}$; **7** is $[B_{10}H_{13}]^-$ where the B(a)–B(c) connectivity is not H-bridged; **8** is [5,6-μ-$\{AuP(C_6H_{11})_3\}B_{10}H_{13}$] where the B(a)–B(c) connectivity is bridged by the $\{AuP(C_6H_{11})_3\}$ function; **9** is $B_{10}H_{13}(SCN)$ where B(a) carries the N-bonded SCN function; **10** is $[B_{11}H_{13}]^{2-}$ (only B_{10} residue considered); **11** is $[B_{11}H_{14}]^-$ (only B_{10} residue considered).

H–C–H 109.47°, and the crystallographic determination was considered sufficiently unreliable that it was necessary to set cage H atoms in idealised positions, B–$H_{terminal}$ 1.15, B–H_{bridge} 1.31–1.36 Å.*

Results and Discussion

1. *R.M.S. Misfit Calculations.*—In this paper we describe the use of the *r.m.s misfit* method in an attempt to identify the extreme fragments *nido*-$\{B_{10}H_{12}\}^{2-}$ and *arachno*-$\{B_{10}H_{12}\}^{4-}$ in a variety of main-group and transition-metal metallaboranes of general formula $[MB_{10}H_{12}]$. The results of such an analysis lead directly to the *formal* oxidation state of the metal atom. Since the method is new it was clearly of importance to check the validity of the results obtained, and we have accomplished this in two ways. The first is to see if the method will clearly distinguish between well known *nido*-$\{B_{10}H_{12}\}^{2-}$ and *arachno*-$\{B_{10}H_{12}\}^{4-}$ fragments, and the second is to make independent measurements of the metal oxidation state wherever possible. The results of the r.m.s. misfit calculations on metallaboranes also lead us to define the 'verticity' of the metal atom, a crude and somewhat arbitrary (but nevertheless useful) measure of the extent to which the metal atom is best regarded as a true cluster vertex.

Calculations between boranes. We have calculated mutual r.m.s. misfits for a number of clusters $B_{10}H_{14}$ **6**,[2] $[B_{10}H_{13}]^-$ **7**,[13,†] [5,6-μ-$\{AuP(C_6H_{11})_3\}B_{10}H_{13}$] **8**[8,14] and $B_{10}H_{13}(SCN)$ **9**,[15] all of which are unambiguously *nido* 10-vertex species. Then we have repeated this process for two boranes that contain the *arachno* B_{10} residue; $[B_{10}H_{14}]^{2-}$ (ref. 16) is clearly an *arachno* 10-vertex borane, but we have not used it as a reference compound since its pattern of μ-H atoms is different to that in **II** and **III**. Instead we have used the $\{B_{10}H_{12}\}$ fragments of the *nido* 11-vertex clusters $[B_{11}H_{13}]^{2-}$ **10**[17] (afforded by removal of the BH unit in the open face which is not involved in H-bridging) and $[B_{11}H_{14}]^-$ **11**[18] (afforded by removal of the BH_2 group), as these fragments have the correct *arachno* geometries *and* the correct pattern of μ-H atoms. Finally we have calculated misfits between **6**, **7**, **8** and **9** as one group, and **10** and **11** as another.

In Table 2 we list (mutual) r.m.s. misfit and individual atom-pair misfits (δ) determined. To overcome the problem of two different numbering schemes for the $\{B_{10}H_{12}\}$ residues of **Ia** and **Ib**, and to avoid any prejudice, all boron atoms have been relabelled B(a)–B(j), corresponding to the generalised metallaborane depicted in **Ic**.

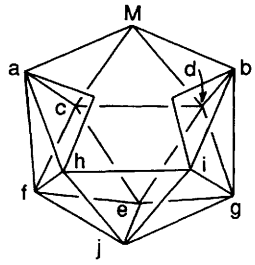

Ic

It is immediately apparent from Table 2 that r.m.s. misfits between like B_{10} clusters (*i.e.* **6**, **7**, **8** and **9** as one group, and **10** and **11** as another) are of the order of 0.06 Å, and that r.m.s. misfits between members of different groups are of the order of 0.18 Å. This clearly opens up the possibility of using the method to distinguish between $\{B_{10}H_{12}\}^{2-}$ and $\{B_{10}H_{12}\}^{4-}$ residues in $[MB_{10}H_{12}]$ metallaboranes, as discussed in the following section.

Inspection of the δ values of Table 2 shows that such differences as do exist between members of one group (first two parts of Table 2) are not always localised to the area of chemical change. In moving from **6** to **7** a (formerly bridging) proton is removed from the B(a)–B(c) connectivity yet the largest δ values occur for B(a) and B(d). In this particular case a partial explanation is afforded by frontier MO considerations. Thus, an EHMO calculation on **7** has previously shown[13] that the HOMO is represented by **IV**, *i.e.* localised on the bonding between B(a) and B(c), with a minor in-phase component on B(d). Depopulation of this orbital (as **7** is protonated to give **6**) thus lengthens the B(a)–B(c) and B(c)–B(d) connectivities, and apparently results in net relative displacements of only B(a) and B(d) (see later for further comment on the structure of **7**). On the other hand the major differences in δ values between **8** and **9** occur for B(b) and B(g), the latter of which is remote from the area of chemical change. Clearly, in such cases the individual δ values are not easily understood, emphasising the importance of *overall* (r.m.s.) misfit values as the best indicator of structural similarity.

* A (narrow) range of B–H–B distances arises as a consequence of the fact that we add μ-H atoms to the borane framework from one side of the bridged connectivity only, using (average) distances, angles and torsions taken from the accurately determined structure of $B_{10}H_{14}$.[2]

† The atom numbering scheme reported in the final three sentences of this paper is unfortunately in error. Atoms B(5), B(6) and B(10) are respectively B(10), B(9) and B(5).

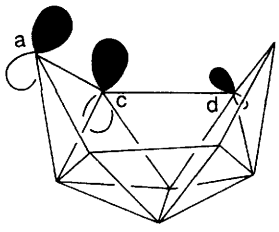

IV

Table 3 (*a*) Root mean square misfits (Å) between metallaboranes *

Complex	1	2	3	4	5	12	13	14	15
2	0.094								
3	0.145	0.058							
4	0.022	0.094	0.143						
5	0.071	0.028	0.076	0.072					
12	0.137	0.047	0.019	0.136	0.068				
13	0.106	0.036	0.049	0.104	0.044	0.053			
14	0.067	0.030	0.072	0.069	0.008	0.080	0.047		
15	0.062	0.043	0.081	0.063	0.022	0.087	0.053	0.019	
16	0.024	0.086	0.129	0.025	0.066	0.136	0.097	0.062	0.057

(*b*) Summary of r.m.s. misfits (Å) between metallaboranes and $B_{10}H_{14}$ **6** or $[B_{11}H_{13}]^{2-}$ **10**, and calculated verticities (%) for metal fragments

Metallaborane	Misfit *vs.* **6**	Misfit *vs.* **10**	Verticity
3	0.150	0.058	73.1
12	0.143	0.067	69.1
13	0.111	0.099	53.0
2	0.105	0.103	50.5
5	0.083	0.124	39.7
14	0.081	0.127	38.4
15	0.074	0.134	34.9
16	0.047	0.183	15.8
1	0.046	0.192	13.3
4	0.034	0.191	10.6

* $[(C_6H_{11})_3PAuB_{10}H_{12}]^-$ **1**, $[(Me_2PhP)_2PtB_{10}H_{12}]$ **2**, $[(Me_2PhP)_3PtB_{10}H_{12}]$ **3**, $[Me_2TlB_{10}H_{12}]^-$ **4**, $[Pt(B_{10}H_{12})_2]^{2-}$ **5**, $[(OC)_3CoB_{10}H_{12}]^-$ **12**, $[(Me_2PhP)_2PtB_{10}H_{11}Cl]$ **13**, $[Pd(B_{10}H_{12})_2]^{2-}$ **14**, $[Ni(B_{10}H_{12})_2]^{2-}$ **15**, $[Zn(B_{10}H_{12})_2]^{2-}$ **16**.

Accepting that an r.m.s. misfit of the order of 0.06 Å represents a measure of the minor differences between two experimental determinations of similar B_{10} residues, then the consistent values of the order of 0.18 Å obtained between the two groups in Table 2 must indicate a more substantial structural change. As previously stated, **6**–**9** are examples of *nido* 10-vertex polyhedra (12 s.e.p.s) whereas **10** and **11** are examples of *arachno* 10-vertex polyhedra (13 s.e.p.s).

The largest individual δ values calculated in the comparison between *nido* and *arachno* B_{10} residues (third part of Table 2) occur for B(a) and B(b), and the reasons for this are discussed subsequently. Also apparent from the data in Table 2 are the consistently greater (by *ca.* 0.03 Å) r.m.s. misfits between *nido* B_{10} cages and **10** ($[B_{11}H_{13}]^{2-}$) than between the same *nido* B_{10} cages and **11** ($[B_{11}H_{14}]^-$). This implies that the B_{10} residue of the latter has a somewhat reduced *arachno* character compared to that of the former. Although we still regard both **10** and **11** as containing *arachno* $\{B_{10}H_{12}\}$ fragments for all practical purposes, this slight difference between them means that we will use the residue of **10** as our model *arachno* B_{10} fragment. In conclusion, therefore, the r.m.s. misfit calculations provide quantitative confirmation that the $\{B_{10}H_{12}\}$ fragment of $B_{10}H_{14}$ **6** is an authentic example of *nido*-$\{B_{10}H_{12}\}^{2-}$, and that the $\{B_{10}H_{12}\}$ fragment of $[B_{11}H_{13}]^{2-}$ **10** is an authentic example of *arachno*-$\{B_{10}H_{12}\}^{4-}$.

Calculations between metallaboranes. In Table 3(*a*) we display r.m.s. misfit values between the B_{10} residues of a variety of metallaboranes, **1**–**5** and $[(OC)_3CoB_{10}H_{12}]^-$ **12**,[19] $[(Me_2PhP)_2PtB_{10}H_{11}Cl]$ **13**,[20] $[Pd(B_{10}H_{12})_2]^{2-}$ **14**,[21] $[Ni(B_{10}H_{12})_2]^{2-}$ **15**[22] and $[Zn(B_{10}H_{12})_2]^{2-}$ **16**,[23] that have been crystallographically characterised. These r.m.s. misfits span the range 0.01–0.15 Å, but the distribution is not bimodal as was the case with the r.m.s. misfits between boranes (Table 2). The greatest misfit in Table 3(*a*) is that between **1** and **3**, telling us that the $\{B_{10}H_{12}\}$ residue of $[(C_6H_{11})_3PAuB_{10}H_{12}]^-$ appears to have a measureably different structure to that in $[(Me_2PhP)_3PtB_{10}H_{12}]$. The r.m.s. misfit calculations between these two metallaboranes and $B_{10}H_{14}$ and $[B_{11}H_{13}]^{2-}$ yield the results (Å) shown below which we interpret in the following

	$B_{10}H_{14}$	$[B_{11}H_{13}]^{2-}$
1 $[(C_6H_{11})_3PAuB_{10}H_{12}]^-$	0.046	0.192
3 $[(Me_2PhP)_3PtB_{10}H_{12}]$	0.150	0.058

simple way: the $\{B_{10}H_{12}\}$ fragment of **1** is best described as *nido*-$\{B_{10}H_{12}\}^{2-}$, whereas that of **3** is best described as *arachno*-$\{B_{10}H_{12}\}^{4-}$.

Thus **3** is a true 11-vertex *nido* metallaborane (structure type **Ia**) in which the platinum atom (formally Pt^{4+}) is an authentic cluster vertex, whilst in **1** the cluster unit is properly defined by only the 10 boron atoms, the role of the gold atom (formally Au^+) being no more than that of a bridge over the B(a)–B(c)–B(d)–B(b) trapezium (structure type **Ib**).

The extent to which the metal fragments in metallaboranes act as true cluster vertices is fundamentally important, and thus we have attempted to quantify the *verticity* (the relative degree of incorporation into the cluster as a vertex) of the metal fragments in all the $[MB_{10}H_{12}]$ metallaboranes studied herein. We define the verticity of the metal fragment in metallaborane **X** by equation (1).

$$\frac{[(\text{r.m.s. misfit } \mathbf{6} \textit{ vs.} \mathbf{10}) + (\text{r.m.s. misfit } \mathbf{X} \textit{ vs.} \mathbf{6}) - (\text{r.m.s. misfit } \mathbf{X} \textit{ vs.} \mathbf{10})] \times 100\%}{2\,(\text{r.m.s. misfit } \mathbf{6} \textit{ vs.} \mathbf{10})} \quad (1)$$

The results obtained* [Table 3(b)] set the metal fragment verticities on an entirely arbitrary scale from low (poor cluster vertex) to high (good cluster vertex). The $\{Pt(PMe_2Ph)_3\}$ and $\{Co(CO)_3\}$ fragments in **3** and **12** are clearly calculated to be good cluster vertices, whilst $\{Zn(B_{10}H_{12})\}$, $\{AuP(C_6H_{11})_3\}$ and $\{TlMe_2\}$ in **16**, **1** and **4** are poor vertices. The metal fragments in **2**, **5** and **13**–**15** all have intermediate verticities, although these appear to fall into two sub-groups, one comprising **2** and **13**, the other **5**, **14** and **15**. Overall there is a *continuum* of verticity. We will subsequently show that these results can be easily understood in terms of the frontier MOs of the various metal fragments.

2. *Metal Oxidation States.*—Formal oxidation states of the metal atoms in metallaboranes follow directly from assignment of the $\{B_{10}H_{12}\}$ fragment as either 2− or 4− from the r.m.s. misfit/verticity calculations. Clearly, an important way of validating the conclusions reached would be to make *independent* measurement of the metal oxidation state where possible. To our knowledge such measurements have not previously been carried out on metallaboranes.

In compound **12** the B_{10} residue is unambiguously $\{B_{10}H_{12}\}^{4-}$ (**III**), leading to the formal metal oxidation state Co^{3+}. Tripositive cobalt ligated by three strongly π-acidic carbonyl ligands is clearly unusual (we can find no other

* These r.m.s. misfits (and hence the metal fragment verticities that follow from them) may in some cases appear slightly different to those previously reported[8,12,19,21] since in the current study, which we regard as definitive, the crystallographically determined structures have been adjusted to full molecular symmetry.

Table 4 XANES absorption edge values

Complex	Absorption edge/eV
12 $[(OC)_3CoB_{10}H_{12}]^{-}$ [a]	13.2
19 $[Co(en)_3]^{3+}$ [b]	13.2
18 $[Co(CO)_3(PPh_3)_2]^{+}$ [c]	10.0

[a] As $[NMe_3(CH_2Ph)]^+$ salt. [b] As tribromide. [c] As $[BPh_4]^-$ salt.

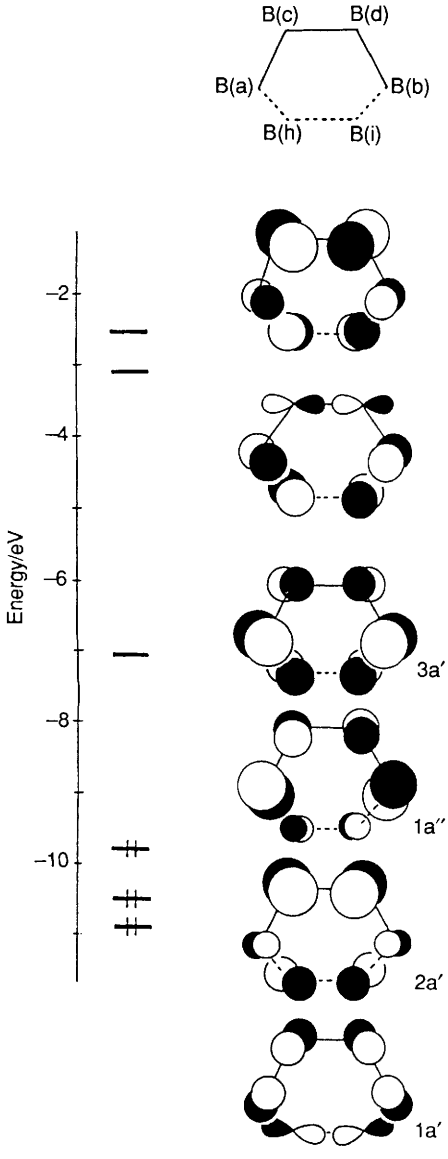

Fig. 1 Frontier molecular orbitals of $\{B_{10}H_{12}\}^{2-}$ **III** viewed perpendicular to the B(a) B(b) B(c) B(d) plane

reference to the $\{(OC)_3Co\}^{3+}$ moiety) so we were particularly interested in establishing the formal metal oxidation state in this compound. To this end we have studied the cation $[Co(CO)_3(dmbd)]^+$ **17** [dmbd = η^4-(2,3-dimethylbutadiene)], a species whose metal oxidation state is obvious (Co^+) and in which the co-ordination sphere around the metal resembles that in **12** in comprising three terminal CO ligands and one (*endo*) acyclic η^4 ligand. Detailed comparison[24] of the molecular structures and carbonyl IR stretching frequencies of **12** and **17** strongly supports a formal metal oxidation state in the former of $>1+$. In addition X-ray absorption near edge structure (XANES) spectra of **12** and of the Co^+ and Co^{3+} standards $[Co(CO)_3(PPh_3)_2]^+$ **18** and $[Co(en)_3]^{3+}$ **19** (en = ethylenediamine) have been recorded, yielding absorption edge values relative to Co foil (Table 4). Overall, therefore, we are confident that these independent studies identify the formal oxidation state of the cobalt atom in **12** as 3+, thereby supporting the conclusion reached *via* the r.m.s. misfit calculations.

In compound **1** the B_{10} residue is unambiguously $\{B_{10}H_{12}\}^{2-}$ (**III**), implying a metal oxidation state Au^+. We have already demonstrated, by Mössbauer spectroscopic study,[8] that compound **1** does indeed contain a formally 1+ gold atom whose co-ordination geometry is essentially linear.

3. *Molecular Orbital Calculations.*—The foregoing discussion uses r.m.s. misfit calculations to analyse the measured molecular geometries of $\{B_{10}H_{12}\}$ fragments of metallaboranes, and thereby to classify the metal fragment of such species as a good cluster vertex, a poor cluster vertex, or something intermediate. In an attempt to understand the conclusions of such an analysis we have performed EHMO–FMO calculations on the metallaboranes **1′**–**3′**, **4** and **5′** partitioning, in each case, the metallaborane as $\{B_{10}H_{12}\}^{2-}$ and the complementary monocationic metal fragment.

The frontier MOs of $\{B_{10}H_{12}\}^{2-}$, **III**, have been described previously[8] and are reproduced, in a view perpendicular to the B(a)–B(c)–B(d)–B(b) trapezium, in Fig. 1. All are outpointing from the trapezoidal face. The 2nd and 3rd highest occupied molecular orbitals (HOMOs) are of a′ symmetry, with the 2nd HOMO in particular being localised on B(c) and B(d). The HOMO is an a″ orbital, and is localised on B(a) and B(b). The lowest unoccupied molecular orbital (LUMO), which is relatively high-lying, is similarly localised but is of a′ symmetry. The broad similarity of this set of MOs to the π-MOs of *cis*-butadiene has already been noted.[8] In **3′** the metal fragment is $\{Ir(PH_3)_3\}^+$, a conical d^8-ML_3 fragment. The metal fragment of **2′** is the angular d^8-ML_2 $\{Ir(PH_3)_2\}^+$, and in **1′** it is the linear d^{10}-ML $\{AuPH_3\}^+$. The frontier MOs of these three fragments are well known[25–27] and are sketched in Fig. 2, together with those of $\{Au(B_{10}H_{12})\}^+$ and $\{TlMe_2\}^+$.

Table 5(*a*) lists the populations of the frontier orbitals (LUMO and 1st–3rd HOMOs) of $\{B_{10}H_{12}\}^{2-}$ in the metallaboranes studied. All five metal fragments whose frontier MOs are presented in Fig. 2 have a radial acceptor orbital of a, or a′ symmetry which causes partial depopulation of the 1a′ and 2a′ orbitals of the borane cage. In the case of **1′** the combined depopulation of 1a′ and 2a′ is substantially greater than the depopulation (by the high-lying gold 6p atomic orbital) of 1a″, confirming that the $\{AuPH_3\}^+$ fragment of **1′**, and by analogy the $\{AuP(C_6H_{11})_3\}^+$ moiety of **1**, acts, essentially, as a one-orbital fragment.[27] In **2′** the depopulation of borane orbitals 1a′ and 2a′ is complemented by that of 1a″ by virtue of its interaction with the metal $1b_1$ acceptor orbital, a 5d–6p hybrid directed towards the trapezoidal face. Interaction of borane 3a′ with metal $1b_2$ is also symmetry-allowed, but is not so effective because the energy separation is greater and this iridium 5d orbital is not hybridised towards the $\{B_{10}H_{12}\}^{2-}$ ligand. In **1′** population of the LUMO of $\{B_{10}H_{12}\}^{2-}$ is effectively zero, and in **2′** it rises to 0.26e. In essence, therefore, the $\{Ir(PH_3)_2\}^+$ fragment of **2′**, and by analogy the $\{Pt(PMe_2Ph)_2\}^{2+}$ fragment of **2**, acts as a source of slightly more than two orbitals for polyhedral bonding.[26]

In contrast, the $\{Ir(PH_3)_3\}^+$ unit of **3′**, and thus the $\{Pt(PMe_2Ph)_3\}^{2+}$ fragment of **3**, acts as a full three-orbital fragment[25] in bonding to the borane—as well as the $1a_1$ metal acceptor orbital causing depopulation of the 1a′ and 2a′ MOs of $\{B_{10}H_{12}\}^{2-}$, the degenerate set 1e enters into two two-orbital two-electron interactions with the borane HOMO and LUMO, substantially depopulating the former and significantly populating (0.77e) the latter.

In **5** the metal fragment verticity is intermediate, but somewhat less than in **2**. Calculations reveal that in **5′** the HOMO of $\{B_{10}H_{12}\}^{2-}$ is efficiently depopulated, but the LUMO carries an insignificant population. Consistent with this the frontier orbitals of the cationic fragment $\{Au(B_{10}H_{12})\}^+$ consist (Fig. 2)

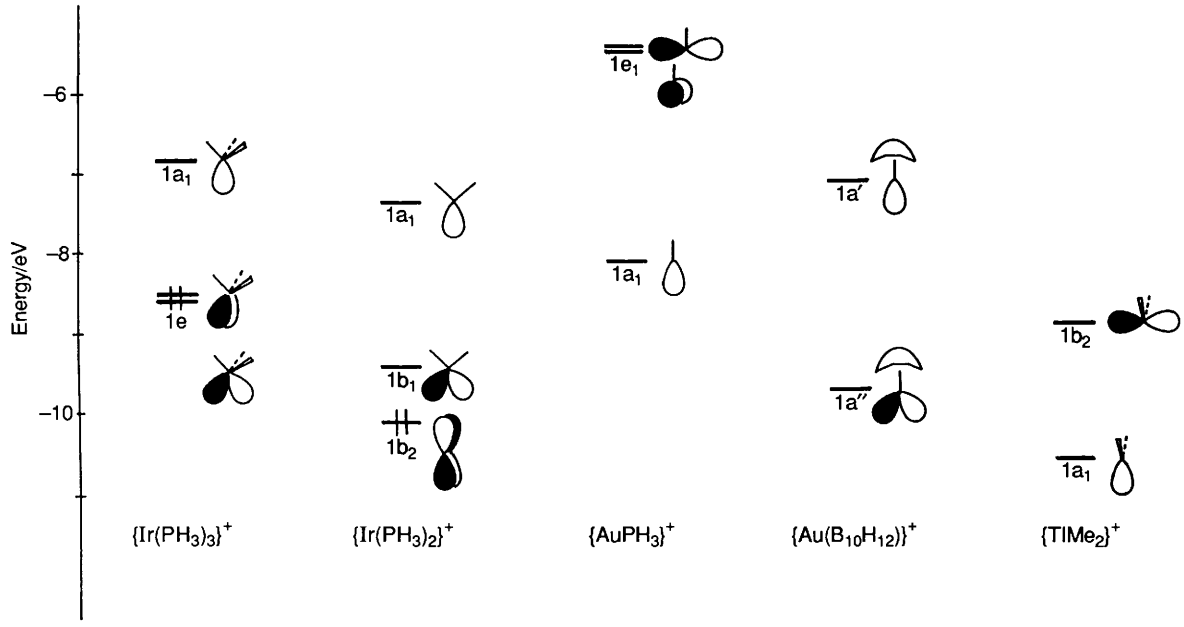

Fig. 2 Frontier molecular orbitals of metal fragments used in the EHMO–FMO calculations

Table 5 (*a*) Populations (e) of the frontier orbitals of $\{B_{10}H_{12}\}^{2-}$ in metallaboranes

Metallaborane	Metal fragment	1a′	2a′	1a″ (HOMO)	3a′ (LUMO)
3′	$\{Ir(PH_3)_3\}^+$	1.800	1.939	1.269	0.766
2′	$\{Ir(PH_3)_2\}^+$	1.773	1.939	1.180	0.260
5′	$\{Au(B_{10}H_{12})\}^+$	1.791	1.895	0.970	0.082
4	$\{TlMe_2\}^+$	1.913	1.647	1.568	0.010
1′	$\{AuPH_3\}^+$	1.826	1.853	1.861	0.054

(*b*) Populations (e) of the frontier orbitals of $\{B_{10}H_{12}\}^{2-}$ in boranes

Borane	Added fragment	1a′	2a′	1a″ (HOMO)	3a′ (LUMO)
6 $B_{10}H_{14}$	$\{H\cdots H\}^{2+}$	1.607	1.585	1.124	0.010
10 $[B_{11}H_{13}]^{2-}$	$\{BH\}$	1.616	1.926	1.157	0.743

* $[H_3PAuB_{10}H_{12}]^-$ **1′**, $[(H_3P)_2IrB_{10}H_{12}]^-$ **2′**, $[(H_3P)_3IrB_{10}H_{12}]^-$ **3′**, $[Me_2TlB_{10}H_{12}]^-$ **4**, $[Au(B_{10}H_{12})_2]^-$ **5′**.

Table 6 Correlation of orbital contribution with verticity of various metal fragments

Metal fragment	Orbital contribution	Verticity (%)
$\{Pt(PMe_2Ph)_3\}^{2+}$	3	73.1
$\{Pt(PMe_2Ph)_2\}^{2+}$	>2	50.5
$\{Pt(B_{10}H_{12})\}$	2	39.7
$\{TlMe_2\}^+$	>1	10.6
$\{AuP(C_6H_{11})_3\}^+$	1	13.3

of an excellent, low-lying acceptor orbital of a″ symmetry as well as the usual, higher-lying, radial orbital (a′). The highest populated metal-based orbital is predominantly gold 5d in character, and thus too low-lying to be useful in bonding. The $\{Au(B_{10}H_{12})\}^+$ fragment, then, appears to be a source of two orbitals for interaction with the second $\{B_{10}H_{12}\}$ moiety, which accounts for the intermediate verticity in **5**. Finally, the $\{TlMe_2\}^+$ fragment of **4** utilises between one and two orbitals for polyhedral bonding; 1a′ and 2a′ of $\{B_{10}H_{12}\}^{2-}$ are depopulated by the $1a_1$ metal-based acceptor orbital, whereas the metal $1b_2$ orbital (thallium 6p) causes only limited depopulation of the borane HOMO since it lies tangential to the cluster surface. The depopulation of 2a′ is unusually efficient because the thallium-based a_1 acceptor orbital is so low-lying. This fact has a second-order effect on the geometry of the $\{B_{10}H_{12}\}$ cage of **4**, and thus on the verticity of the $\{TlMe_2\}^+$ fragment, as discussed later.

Describing the orbital contribution of the various metal fragments in this (localised) way is useful because it establishes a simple and clear rationale for the verticities established by the r.m.s. misfit calculations—*to a first approximation, the greater the orbital contribution of the metal fragment the greater is its ability to function as a good cluster vertex, i.e. the greater its verticity*, as detailed in Table 6. Of the various metal fragments in this tabulation only $\{Pt(PMe_2Ph)_3\}^{2+}$ is isolobal with $\{BH\}$, the archetypal good cluster vertex. Indeed, an EHMO–FMO calculation on $[B_{11}H_{13}]^{2-}$ reveals that the population of the LUMO of the $\{B_{10}H_{12}\}^{2-}$ sub-cluster [Table 5(*b*)] is 0.74e, essentially the same as in $[(Me_2PhP)_3PtB_{10}H_{12}]$.

Clearly, on the basis of the above simple analysis the $\{TlMe_2\}$ fragment should have a greater verticity than that of $\{AuP(C_6H_{11})_3\}$ but does not. As noted, however, the depopulation of 2a′ of $\{B_{10}H_{12}\}^{2-}$ in **4** is unusually high, and we will subsequently argue that this fact is directly responsible for the 'anomalous' low verticity of $\{TlMe_2\}^+$.

4. *Relationship between R.M.S. Misfit Calculations, Orbital Populations and Other Molecular Parameters.—Oxidation state.* The results described above show that the continuum of verticity displayed by metal fragments in metallaboranes is directly related to the similar continuum of number of valence orbitals the various metal fragments have available for polyhedral (metal–borane) bonding. We have established that in metallaboranes **1′**, **4** and **5′** there is minimal population of the

Table 7 B(a)···B(b) and B(c)–B(d) distances (Å) and metal fragment vertices (%) in boranes and metallaboranes

Compound	B(a)···B(b)	B(c)–B(d)	Verticity
9 $B_{10}H_{13}(SCN)$	3.591	1.983	
6 $B_{10}H_{14}$	3.590	1.988	
8 $[5,6\text{-}\mu\{AuP(C_6H_{11})_3B_{10}H_{13}]$	3.563	1.999	
1 $[(C_6H_{11})_3PAuB_{10}H_{12}]^-$	3.551	1.902	13.3
4 $[Me_2TlB_{10}H_{12}]^-$	3.541	1.967	10.6
16 $[Zn(B_{10}H_{12})_2]^{2-}$	3.494	1.936	15.8
7 $[B_{10}H_{13}]^-$	3.462	1.848	
15 $[Ni(B_{10}H_{12})_2]^{2-}$	3.392	1.870	34.9
14 $[Pd(B_{10}H_{12})_2]^{2-}$	3.352	1.825	38.4
5 $[Pt(B_{10}H_{12})_2]^{2-}$	3.347	1.825	39.7
2 $[(Me_2PhP)_2PtB_{10}H_{12}]$	3.239	1.818	50.5
13 $[(Me_2PhP)_2PtB_{10}H_{11}Cl]$	3.234	1.850	53.0
12 $[(OC)_3CoB_{10}H_{12}]^-$	3.136	1.788	69.1
3 $[(Me_2PhP)_3PtB_{10}H_{12}]$	3.115	1.819	73.1
11 $[B_{11}H_{14}]^-$	3.059	1.765	
10 $[B_{11}H_{13}]^{2-}$	2.914	1.765	

LUMO of $\{B_{10}H_{12}\}^{2-}$, which is entirely consistent with the B_{10} residues of metallaboranes **1**, **4** and **5** being formally described *as* $\{B_{10}H_{12}\}^{2-}$, line structure **III**. In contrast, the LUMO of $\{B_{10}H_{12}\}^{2-}$ in **3'** is substantially populated (0.77e), consistent with the B_{10} residue of **3** being formally represented by $\{B_{10}H_{12}\}^{4-}$, **II**. The metal fragments in both **3** and **12** have high verticities (as would be expected since $\{Co(CO)_3\}^+$ is isolobal with $\{Pt(PMe_2Ph)_3\}^{2+}$), so the B_{10} residue in **12** is also $\{B_{10}H_{12}\}^{4-}$. From these extreme representations of the B_{10} sub-cluster follow formal metal oxidation states of 1+ in **1**, 3+ in **4**, 2+ in **5**, 4+ in **3** and 3+ in **12**. For **1** and **12** these conclusions are in good accord with independent measurement.

How does one similarly interpret the results obtained for $[(Me_2PhP)_2PtB_{10}H_{12}]$ **2**? In **2'** the LUMO of $\{B_{10}H_{12}\}^{2-}$ is not empty (0.26e) but neither is it substantially populated. In cases like **2** (and **13**) it is clearly impossible formally to classify the B_{10} residues as either **II** or **III**, or therefore to assign any integer value to the platinum oxidation state. It appears to be, effectively, somewhat greater than +2, but not much greater. This interpretation is not inconsistent with previous views of the metal–borane bonding in **2** by Kennedy and co-workers[1,9] who describe, in localised orbital terms, 'contributions from PtB(c)B(d) three-centre bonding and concomitant platinum 4+ character'. There has, however, been occasional confusion[9,28] about precisely which orbitals of a d^8-ML_2 fragment are involved in cluster bonding. Clearly the two primary metal orbitals used in this connection are $1a_1$ and $1b_1$ (Fig. 2). The secondary metal orbital is d_{yz} and not d_{z^2} (assuming ML_2 in the *xz* plane), since only the former is of the correct symmetry to interact with the borane LUMO.

Molecular geometry. We have seen that the frontier orbitals of $\{B_{10}H_{12}\}^{2-}$ are localised predominantly on B(a), B(b), B(c) and B(d). These atoms are related in pairs across the mirror plane of symmetry of $\{B_{10}H_{12}\}$, and since the a' and a'' borane orbitals are distinguished by the absence or presence of a nodal plane coincident with this symmetry plane it is informative to consider trends in interatomic distances that are normal to the plane, *viz.* B(a)···B(b) and B(c)–B(d). The basic expectations based on changes in orbital population may be summarised as follows (normal type, minor effect; italic type, major effect):

Orbital change	B(a)···B(b)	B(c)–B(d)
1a' Depopulated	Lengthens	Lengthens
2a' Depopulated	Lengthens	*Lengthens*
1a'' Depopulated	*Shortens*	Shortens
3a' Populated	*Shortens*	Shortens

Table 7 compiles B(a)···B(b) and B(c)–B(d) distances (symmetry-adjusted) for all the boranes and metallaboranes considered in this paper, in order of decreasing B(a)···B(b). There are three important points that arise from this compilation.

First, examples of boranes containing the *nido* $\{B_{10}H_{12}\}^{2-}$ residue (**6**–**9**) are well separated from those containing *arachno* $\{B_{10}H_{12}\}^{4-}$ (**10** and **11**) in terms of both B(a)···B(b) and B(c)–B(d), but predominantly in the former. Table 5(*b*) shows that the essential changes in population of the orbitals of $\{B_{10}H_{12}\}^{2-}$ in going from $B_{10}H_{14}$ to $[B_{11}H_{13}]^{2-}$ are (*i*) less depopulation of 2a' and (*ii*) substantial population of 3a'. The former arises because the a_{1g} acceptor orbital of the $\{H\cdots H\}^{2+}$ fragment is much lower-lying than the a_1 acceptor orbital * of {BH}, and this is the main cause of the longer (by *ca.* 0.2 Å) B(c)–B(d) distance in $B_{10}H_{14}$ and its simple derivatives. The latter has a major effect on the B(a)···B(b) distance, 0.5–0.6 Å shorter in **10** and **11** than in **6**–**9**. Recall that the largest individual δ values in the third part of Table 2 are for B(a) and B(b).

Secondly, within the metallaboranes the sequence of decreasing B(a)···B(b) distance follows that of increasing verticity of the metal fragment, except that **1** and **4** are interchanged. To a first approximation all metal fragments cause partial depopulation of the 1a' and 2a' orbitals of $\{B_{10}H_{12}\}^{2-}$. Two-orbital sources additionally depopulate 1a'', and three-orbital sources further cause population of 3a'. The major effect of both these last two changes is to shorten B(a)···B(b), hence the observed pattern in B(a)···B(b) distance as a function of verticity. Note that the relationship between verticity and B(a)···B(b) distance is much more pronounced than that between verticity and B(c)–B(d) distance. Thus, as a crude preliminary indication of the extent of interaction between metal fragments and $\{B_{10}H_{12}\}^{2-}$, B(a)···B(b) is a much better guide than B(c)–B(d).

As previously noted, the low-lying $1a_1$ acceptor orbital of the $\{TlMe_2\}^+$ fragment causes unusually efficient depopulation of 2a' of $\{B_{10}H_{12}\}^{2-}$, almost to the level attained in $B_{10}H_{14}$ [the strength of this interaction is a consequence of the fact that the thallium a_1 orbital points almost directly towards the B(c)–B(d) midpoint]. This results in a long B(c)–B(d) distance (as far as we are aware the longest yet reported in a $[MB_{10}H_{12}]$ metallaborane) and a small r.m.s. misfit between the B_{10} residue of **4** and $B_{10}H_{14}$. Thus, although the $\{TlMe_2\}^+$ fragment clearly interacts more strongly with $\{B_{10}H_{12}\}^{2-}$ than does $\{AuP(C_6H_{11})_3\}^+$ [compare the depopulations of 2a' and 1a'' in Table 5(*a*)], its verticity is calculated to be lower. In view of this 'anomaly' it is unfortunate that so few similar main-group $[MB_{10}H_{12}]$ species have been structurally characterised.[1] It may ultimately be necessary to establish separate verticity scales for main-group and transition-metal fragments in metallaboranes.

Thirdly, the metallaborane entries in Table 7 all fall between those boranes containing the $\{B_{10}H_{12}\}^{2-}$ fragment and those containing $\{B_{10}H_{12}\}^{4-}$, except that in $[B_{10}H_{13}]^-$ the B(a)···B(b) distance is shorter than in those metallaboranes in which the metal fragment verticity is lowest. Thus even the worst (in terms of verticity) metallaborane is not as decaborane-like as decaborane itself, whilst at the other end of the scale even the best metal vertex does not cause the B(a)···B(b) distance to shorten as much as does {BH}. Table 5(*b*) shows that the combined depopulation of 1a' and 2a' of $\{B_{10}H_{12}\}^{2-}$ by the fragment $\{H\cdots H\}^{2+}$ (in $B_{10}H_{14}$) is as efficient as the depopulation of 1a''. For none of the metallaboranes (with the possible exception of **4**, the most decaborane-like) is this the

* Formally, the radial a_1 orbital of {BH} is populated and the e_1 pair (B $2p_x$, $2p_y$) is empty in the ground state, so to describe the former as an acceptor orbital might appear surprising. However, this partitioning of electrons becomes irrelevant when {BH} bonds to $\{B_{10}H_{12}\}^{2-}$ to afford **10** since only the a_1 orbital is of the correct symmetry to interact with the filled a' borane orbitals, and one component of the e_1 pair is the only orbital of suitable symmetry to match with the borane LUMO.

case, presumably because the radial metal-acceptor orbitals are relatively high-lying. Since depopulation of the 1a′ and 2a′ orbitals of $\{B_{10}H_{12}\}^{2-}$ lengthens B(a)···B(b) [and B(c)–B(d)], longer distances result in decaborane and its simple derivatives. The borane $[B_{10}H_{13}]^-$ has much shorter B(a)···B(b) and B(c)–B(d) distances because the a′ depopulation by only one proton is naturally less. The fact that the B(a)···B(b) [and B(c)–B(d)] distances in **10** and **11** are somewhat shorter than those in high-verticity $[MB_{10}H_{12}]$ species cannot be explained in terms of orbital populations, since the populations of the frontier orbitals of $\{B_{10}H_{12}\}^{2-}$ are practically the same in **3′** and **10**.* The likely explanation is simply that since the radial characteristics of the frontier orbitals of metal fragments are greater than those of {BH}, maximum overlap between metal vertex and borane orbitals is achieved with a more open B(a)B(c)B(d)B(b) face.† Such a factor would become increasingly important as the non-radial metal fragment orbitals became more involved, as they do in metallaboranes at the high verticity end of the scale.

The combined consequence of the two factors described above is that metal fragment verticities in metallaboranes are unlikely ever to be extremely high (~100%) or extremely low (~0%). One could stretch the verticity scale by, *e.g.*, using **1** and **3** instead of **6** and **10** in the equation for calculating verticity, but until such time as the current system is shown to be seriously deficient we would argue in favour of retention of the present method.

Conclusion

Application of *r.m.s. misfit* calculations to metallaboranes of the type $[MB_{10}H_{12}]$ has identified clear examples of both $\{B_{10}H_{12}\}^{2-}$ and $\{B_{10}H_{12}\}^{4-}$ ligands. In the former case the ligated metal atom is not considered a true cluster vertex, whereas in the latter case it is. The term *verticity* is introduced in an attempt to quantify the degree of incorporation of the metal into the cluster as a vertex. A continuum of verticity exists and is shown to be related, to a first approximation, to a continuum (between one and three) in the number of valence orbitals the metal fragment uses in polyhedral bonding.

Root mean square misfit calculations can be applied to any pair of similar molecules for which atomic coordinates are available, allowing the similarity to be quantified, both as individual (atom pair) and as an overall (r.m.s.) misfit.[30] Clearly such calculations are highly appropriate to cluster compounds, in which there is often an unmanageable number of potential parameters (bond lengths, interbond angles, torsion angles) with which to attempt to quantify similarity in a conventional way, and in this respect we have already demonstrated the usefulness of these calculations in distinguishing between two types of $\{Au_2B_8H_{10}\}$ framework.[31] Future contributions will further exploit the potential of r.m.s. misfit calculations in understanding the structures of other polyboron compounds and other cluster systems.

* The populations of the orbitals of $\{B_{10}H_{12}\}^{2-}$ are also practically the same for **2′** and **11** which contain, respectively, the isolobal fragments $\{Ir(PH_3)_2\}^+$ and $\{BH_2\}$. For **11** the populations (e) are 1a′ 1.704, 2a′ 1.938, 1a″ 1.313 and 3a′ 0.308.

† Support for this idea can be found in a number of metalla(hetero)-borane structures. Consider, *e.g.*, the very accurately determined structure of $[3\text{-}(\eta\text{-}C_9H_7)\text{-}3,1,2\text{-}CoC_2B_9H_{11}]$.[29] In this molecule the cobalt atom and B(6) both cap C_2B_3 faces, the sides of which average 1.7320 and 1.7145 Å respectively, with the maximum estimated standard deviation on an individual connectivity being 0.0024 Å.

Acknowledgements

We thank the SERC for support of S. A. Macgregor, A. J. Wynd and P. Taylor. Dr. M. Thornton-Pett (University of Leeds) is thanked for supplying several sets of atomic fractional co-ordinates prior to publication. The synthesis by the Edinburgh group of several metallaboranes analysed here has been greatly facilitated by a loan of precious metals from Johnson Matthey, and by a generous gift of decaborane from the Callery Chemical Co. Independent measurement of metal oxidation states in metallaboranes has been crucial in validating conclusions reached by the r.m.s. misfit method, and for this we thank Dr. R. V. Parish (UMIST) for Mössbauer spectroscopic studies, and Patricia M. Mackel and Professor C. D. Garner (University of Manchester) for XANES studies.

References

1 J. D. Kennedy, *Prog. Inorg. Chem.*, 1986, **34**, 211.
2 R. Brill, H. Dietrich and H. Dierks, *Acta Crystallogr., Sect. B*, 1971, **27**, 2003.
3 K. Wade, *Chem. Commun.*, 1971, 792.
4 See, for example, R. T. Baker, *Inorg. Chem.*, 1986, **25**, 109; J. D. Kennedy, *Inorg. Chem.*, 1986, **25**, 111; R. L. Johnson and D. M. P. Mingos, *Inorg. Chem.*, 1986, **25**, 3321.
5 R. Hoffmann, *J. Chem. Phys.*, 1963, **39**, 1397.
6 J. Howell, A. Rossi, D. Wallace, K. Haraki and R. Hoffmann, ICON8, Quantum Chemistry Programme Exchange, University of Indiana, 1977, no. 344.
7 J. H. Ammeter, H.-B. Burgi, J. C. Thibault and R. Hoffmann, *J. Am. Chem. Soc.*, 1982, **100**, 3686.
8 A. J. Wynd, A. J. Welch and R. V. Parish, *J. Chem. Soc., Dalton Trans.*, 1990, 2185.
9 S. K. Boocock, N. N. Greenwood, J. D. Kennedy, W. S. McDonald and J. Staves, *J. Chem. Soc., Dalton Trans.*, 1981, 2573.
10 M. Thornton-Pett, personal communication.
11 N. N. Greenwood and J. A. Howard, *J. Chem. Soc., Dalton Trans.*, 1976, 177.
12 S. A. Macgregor, L. J. Yellowlees and A. J. Welch, *Acta Crystallogr., Sect. C*, 1990, **46**, 1399.
13 A. J. Wynd and A. J. Welch, *Acta Crystallogr., Sect. C*, 1989, **45**, 615.
14 A. J. Wynd, A. J. McLennan, D. Reed and A. J. Welch, *J. Chem. Soc., Dalton Trans.*, 1987, 2761.
15 D. S. Kendall and W. N. Lipscomb, *Inorg. Chem.*, 1973, **12**, 2915.
16 D. S. Kendall and W. N. Lipscomb, *Inorg. Chem.*, 1973, **12**, 546.
17 C. J. Fritchie, *Inorg. Chem.*, 1967, **6**, 1199.
18 T. D. Getman, J. A. Krause and S. G. Shore, *Inorg. Chem.*, 1988, **27**, 2398.
19 S. A. Macgregor, L. J. Yellowlees and A. J. Welch, *Acta Crystallogr., Sect. C*, 1990, **46**, 551.
20 J. E. Crook, N. N. Greenwood, J. D. Kennedy and W. S. McDonald, *J. Chem. Soc., Dalton Trans.*, 1984, 2487.
21 S. A. Macgregor, J. A. Scanlan, L. J. Yellowlees and A. J. Welch, *Acta Crystallogr., Sect. C*, 1991, **47**, 513.
22 L. J. Guggenberger, *J. Am. Chem. Soc.*, 1972, **94**, 114.
23 N. N. Greenwood, J. A. McGinnety and J. D. Owen, *J. Chem. Soc. A*, 1971, 809.
24 S. A. Macgregor, L. J. Yellowlees and A. J. Welch, *Acta Crystallogr., Sect. C*, 1991, **47**, 536.
25 M. Elian, M. M. L. Chen, D. M. P. Mingos and R. Hoffmann, *Inorg. Chem.*, 1976, **15**, 1148.
26 D. M. P. Mingos, *J. Chem. Soc., Dalton Trans.*, 1977, 602.
27 D. G. Evans and D. M. P. Mingos, *J. Organomet. Chem.*, 1982, **232**, 171.
28 M. A. Beckett, J. E. Crook, N. N. Greenwood and J. D. Kennedy, *J. Chem. Soc., Dalton Trans.*, 1984, 1427.
29 D. E. Smith and A. J. Welch, *Organometallics*, 1986, **5**, 760.
30 See, for example, J. Cowie, E. J. M. Hamilton, J. C. V. Laurie and A. J. Welch, *Acta Crystallogr., Sect. C*, 1988, **44**, 1648.
31 A. J. Wynd and A. J. Welch, *J. Chem. Soc., Dalton Trans.*, 1990, 2803.

Received 20*th June* 1991; *Paper* 1/03056F